References

DAVID, W. I. F., JOHNSON, M. W. & WILSON, C. C. (1988). *Mater. Sci. Forum*, **27/28**, 49-62.
GILMORE, C. J. (1984). *J. Appl. Cryst.* **17**, 42-46.
JOHNSON, M. W. & DAVID, W. I. F. (1985). Report RAL-85-112. Rutherford Appleton Laboratory, Didcot, Oxon, England.
KARLE, J. (1968). *Acta Cryst.* B**24**, 182-186.
LOW, J. N. & WILSON, C. C. (1983). *Acta Cryst.* C**39**, 1688-1690.
MAIN, P. (1976). In *Crystallographic Computing Techniques*, edited by F. R. AHMED, K. HUML & B. SEDLACEK, pp. 97-105. Munksgaard: Copenhagen.
NELMES, R. J., TUN, Z., DAVID, W. I. F. & HARRISON, W. T. A. (1987). In *Chemical Crystallography with Pulsed Neutrons and Synchrotron Radiation*, edited by M. A. CARRONDO & G. A. JEFFREY, p. 479. Proc. of NATO ASI.
SEMMINGSEN, D., HOLLANDER, F. J. & KOETZLE, T. F. (1977). *J. Chem. Phys.* **66**, 4405.
TOLLIN, P. (1966). *Acta Cryst.* **21**, 613-614.
TOLLIN, P. & COCHRAN, W. (1964). *Acta Cryst.* **17**, 1322-1324.
WADSWORTH, J. W., WILSON, C. C. & DAVID, W. I. F. (1989). *Nucleosides Nucleotides*, **8**, 537-547.
WILSON, C. C. (1987). Report RAL-87-060. Rutherford Appleton Laboratory, Didcot, Oxon, England.
WILSON, C. C. (1988). Report RAL-88-087. Rutherford Appleton Laboratory, Didcot, Oxon, England.
WILSON, C. C., LOW, J. N. & TOLLIN, P. (1985). *Acta Cryst.* C**41**, 1123-1125.
WILSON, C. C. & TOLLIN, P. (1986). *J. Appl. Cryst.* **19**, 411-412.
WILSON, C. C. & TOLLIN, P. (1988). *Acta Cryst.* A**44**, 226-230.

Acta Cryst. (1989). A**45**, 839-851

Three-Beam and Many-Beam Theory in Electron Diffraction and its Use for Structure-Factor Phase Determination in Non-centrosymmetric Crystal Structures

BY J. M. ZUO

Department of Physics, Arizona State University, Tempe, AZ 85287, *USA*

R. HØIER

Department of Physics, University of Trondheim-NTH, 7034 *Trondheim, Norway*

AND J. C. H. SPENCE

Department of Physics, Arizona State University, Tempe, AZ 85287, *USA*

(*Received* 28 *February* 1989; *accepted* 1 *August* 1989)

Abstract

Closed-form expressions for three-beam dynamical transmission electron diffraction are compared. These are used as a guide to determine the best experimental conditions for the determination of structure-factor phases by convergent-beam electron diffraction in the general non-systematic case. The validity domains of Kambe's [*J. Phys. Soc. Jpn* (1957), **12**, 1-13] 'strong coupling' approximation and Bethe's [*Ann. Phys. (Leipzig)* (1928), **87**, 55-129] second approximation are compared, and these approximations reconciled. A comparison of many-beam calculations with experimental non-systematic CBED patterns is used to determine a three-phase invariant for CdS with an accuracy of $\pm 5°$ in the electron structure-factor phase. If it is assumed that two of the phases are known exactly, the error in the third $(00\bar{2})$ X-ray structure-factor phase would be $\pm 0{\cdot}75°$. The accuracy of the method for determining phases, atomic position parameters and bonding charge distributions is discussed.

1. Introduction

In the 60 years which have passed since the discovery of the diffraction of electrons by crystals there have been many attempts to extract crystal structure and bonding information from electron diffraction patterns [for a review, see Cowley (1981)]. Unlike X-rays, except for special cases, the much stronger interaction of electrons with matter renders the intensity of the multiply scattered electron beams very sensitive to the phases of crystal structure factors. The two-beam dynamical theory, however, does not preserve structure-factor phase information. In his classic study of three-beam dynamical electron diffraction, K. Kambe showed that the dynamical intensity depends on the sum of the phases of the three structure factors involved in the interaction, which is called the three-phase structure invariant (Kambe, 1957). Fourteen years later it was shown for the same non-systematic three-beam case that a degeneracy point exists at which the intensity is zero for centrosymmetric crystals (Gjønnes & Høier, 1971). The position

0108-7673/89/120839-13$03.00

of this point indicates immediately whether the three-phase structure invariant sums to 0 or π. Methods of determining both amplitudes and phases in centrosymmetric crystals have been described, which depend on finding lines in a three-beam pattern along which the intensity expression reduces to two-beam form (Hurley & Moodie, 1980). The application of similar three-beam effects in X-ray crystallography has been reviewed recently (Chang, 1987).

Work on the general phase problem in electron diffraction has a long history (Fues, 1949; Miyake & Uyeda, 1955; Kambe, 1957). For non-centrosymmetric (acentric) crystals, however, detailed theoretical work has only recently begun (Marthinsen & Høier, 1986; Bird, James & Preston, 1987; Marthinsen, Matsuhata, Høier & Gjønnes, 1988. A very few applications to transmission electron diffraction (Høier, Zuo, Marthinsen & Spence, 1988; Zuo, Spence & Høier, 1989) and channelling (Marthinsen & Høier, 1988) have also appeared.

Since the theory of dynamical electron diffraction by crystals has been well understood for many years [see Humphreys (1979) for a review], and efficient algorithms exist for its computer implementation, it is perhaps surprising that no general methods for crystal structure determination by electron diffraction currently exist. In addition to 'solving' the phase problem inherent in all diffraction problems, convergent-beam electron microdiffraction (CBED) also allows the quantitative recording of single-crystal patterns from fine-grained polycrystalline and multiphase samples, since a focused electron probe only a few nanometres in diameter can be used on modern electron microscopes. This greatly expands the range of real materials, rather than synthetic analogues, which can be studied. The development of electron microscopes with higher vacuum (and thus reduced contamination), improved beam-current stability for longer recording times, and reduced aberrations have all contributed to these advances. The use of cooled charge-coupled device parallel detection arrays with large dynamic range also assists quantitative work (Spence & Zuo, 1988). Finally, the ability to form high-resolution electron microscope images of the region used to form the diffraction pattern allows regions to be sought for analysis which are free of line or planar defects, strain and chemical inhomogeneities.

The reasons for this lack of progress in quantitative electron diffraction, despite its apparent promise, are not difficult to find. The essential problem is to find a strategy or systematic procedure for the analysis of a crystal of unknown structure. As a contribution to the development of such methods, in this paper we consider both approximate analytical methods, and full dynamical calculations in acentric structures in general, and application to a particular structure with a single positional parameter. So far, refinement by direct dynamical computation and least-squares many-parameter fitting has not proved a realistic possibility. For a typical small-unit-cell crystal, a 50-beam dynamical Bloch-wave calculation performed on a VAX750 takes about 1 min for each plane-wave component of the incident wave packet, for a single set of refinement parameters (Zuo, Spence & O'Keeffe, 1988). These parameters include the electron structure factors V_g (or atomic position parameters u_i), absorption coefficients, sample thickness, accelerating voltage and Debye-Waller factors. Most of the time is occupied in diagonalizing a complex non-Hermitian matrix. Computing times for the multislice method are not greatly different. No angular perturbation theory has yet been produced to speed these calculations by relating calculations for slightly different incident directions. Since thousands of points are required to simulate a general two-dimensional zero-order Laue zone (ZOLZ) pattern for each set of refinement parameters, we see that the direct matching of experimental and computed whole patterns is not practical at present. This situation is now changing rapidly with advances in the new supercomputers.

For particular cases, however, some impressive successes have been achieved. The most accurate value for the 200 reflection in GaAs has been obtained by the CBED method (Zuo, Spence & O'Keeffe, 1988). Bonding effects have been measured in several crystals of known structure (Voss, Lehmpfuhl & Smith, 1980; Goodman, 1976; Smart & Humphreys, 1978; Shishido & Tanaka, 1976). The critical voltage method has also been used to give accurate structure factors in many cases [see Fox & Fisher (1988) and Sellar, Imeson & Humphreys (1980)], while the more versatile but somewhat less accurate intersecting Kikuchi line method has proven useful for small crystals which are difficult to study by other methods (Høier & Anderson, 1974; Taftø & Gjønnes, 1985; Matsuhata, Tomokiyo, Watanabe & Eguchi, 1984). The structure of an unknown microphase has even been solved from CBED intensity data (Vincent, Bird & Steeds, 1984).

Since whole-pattern matching is not feasible at present, the question arises as to which portions of the CBED pattern are most sensitive to changes in atomic position parameters and ionicity, and which choice of specimen thickness gives the greatest sensitivity. For acentric crystals, an expression for the minimum dispersion surface gap has been given (Marthinsen, Matsuhata, Høier & Gjønnes, 1988), and the sensitivity of the corresponding features in CBED patterns to the three-phase invariant has been discussed. Our experience with numerical simulations also suggests some answers to these questions. The purpose of this paper then is to compare the various three-beam approximations for acentric crystals, and to use them to determine the accuracy with which

position parameters can be extracted from experimental data. Many-beam calculations for 'three-beam' orientations are also reported, concentrating on the degeneracy point which is most sensitive to structure-factor phase. In this way we aim to develop a strategy for quantitative electron crystallography. An application to phase determination in CdS is also given, and the accuracy of the method assessed. Position-parameter determination in CdS is briefly discussed.

Techniques for reducing many-beam cases in orientations of high symmetry to two- or three-beam form have been described in the literature (*e.g.* Kogiso & Takahashi, 1977). These 'beam reduction' methods can only supply data along lines of symmetry in each disc, and are therefore not useful for our purposes.

We first note that the phase of the electron 'structure factor' V_g (or U_g) is not equal to that of the corresponding X-ray structure factor $F^x(s)$, and no simple relation between them is found in the general case. They are related by the Motte-Bethe formula, which gives, for crystal atoms of atomic number Z_i and atomic scattering factor $f_i^x(s)$

$$V_g = (1{\cdot}1459123/\Omega) \times \sum_i \{[Z_i - f_i^x(s)]/s^2\} \exp(-2\pi i \mathbf{g}.\mathbf{r}_i). \quad (1)$$

However, the phase of the X-ray structure factor is determined by

$$F_g = \sum_i f_i^x(s) \exp(-2\pi i \mathbf{g}.\mathbf{r}_i).$$

Here $s = (\sin\theta)/\lambda$, with λ relativistically corrected, and θ the Bragg angle. $f^x(s)$ is dimensionless, V_g is given in volts and the sum is over a unit cell of volume Ω (Å^3). The quantities U_g (in Å^{-2}) used in the dynamical theory which follows are given by

$$U_g = 2m|e|V_g/h^2. \quad (2)$$

Since m is relativistically corrected, the amplitude but not the phase of U_g depends on accelerating voltage. In acentric crystals without absorption corrections $U_g = U^*_{-g}$. The sign convention adopted above and throughout this paper is consistent with an incident plane wave of the form $\exp(+2\pi i \mathbf{k}_0.\mathbf{r})$ (Saxton, O'Keeffe, Cockayne & Wilkens, 1983). Equation (1) expresses Poisson's equation in the Fourier domain. Thus, for small Bragg angles θ, small changes in the Fourier coefficients of electronic charge density F_g have a large effect on V_g, the coefficients of potential (Cowley, 1953).

We devote the next three theory sections to summaries and development of the current state of knowledge of general three-beam solutions and approximations. We then discuss, in the light of these results, the choice of experimental conditions which renders the diffracted intensities most sensitive to crystal structure and bonding. Since we are concerned with elastic scattering, we do not make the independent-Bloch-wave approximation which is appropriate for inelastic scattering, or assume that the contrast (width) of features in the Kikuchi lines is proportional to the width of the gap at the dispersion surface (Gjønnes & Høier, 1971). The final section applies these ideas to the case of the one-parameter structure CdS in order to assess the error in a measurement of this parameter and phase by electron diffraction.

2. Exact solution for centrosymmetric crystals

The general expression for the total wave amplitude inside a thin crystal of thickness t traversed by a collimated kilovolt electron beam in the Bloch-wave formulation of dynamical theory is (Humphreys, 1979)

$$\Psi(\mathbf{r}, \mathbf{K}_t) = \sum_i \alpha_i \sum_{\mathbf{g}} C_{\mathbf{g}}^i \exp(2\pi i \gamma^i z) \exp[2\pi i(\mathbf{K}+\mathbf{g}).\mathbf{r}]. \quad (3)$$

Here γ^i are the eigenvalues of the dispersion equation (5) below and $\mathbf{K}_t$ is the tangential component of $\mathbf{K}$. $\mathbf{K}$ is defined in (7), z is taken parallel to the beam direction and normal to the surface, and the C_g are eigenvector elements. Boundary conditions appropriate to a thin parallel-sided slab of crystal give $\alpha_i = C_0^{i*}$, and we make the projection approximation [neglect of reflections in higher-order Laue zones (HOLZ)]. We assume that the incident-beam direction is close to the surface-normal direction. In the absence of absorption, the amplitude of a particular Bragg beam $\mathbf{g}$ at the exit surface where $z = t$ is

$$\Phi_{\mathbf{g}} = \exp[2\pi i(\mathbf{K}+\mathbf{g}).\mathbf{r}] \sum_i C_0^{i*} C_{\mathbf{g}}^i \exp(2\pi i \gamma^i t). \quad (4)$$

The three-beam dispersion equation for beams $\mathbf{0}$, $\mathbf{h}$ and $\mathbf{g}$ which results from solving the Schrödinger equation using Bloch waves is

$$\begin{bmatrix} 0 & U_{-\mathbf{g}} & U_{-\mathbf{h}} \\ U_{\mathbf{g}} & 2KS_{\mathbf{g}} & U_{\mathbf{g}-\mathbf{h}} \\ U_{\mathbf{h}} & U_{\mathbf{h}-\mathbf{g}} & 2KS_{\mathbf{h}} \end{bmatrix} \begin{bmatrix} C_0 \\ C_{\mathbf{g}} \\ C_{\mathbf{h}} \end{bmatrix} = 2K\gamma \begin{bmatrix} C_0 \\ C_{\mathbf{g}} \\ C_{\mathbf{h}} \end{bmatrix}. \quad (5)$$

The excitation error $S_{\mathbf{g}}$ for reflection $\mathbf{g}$ is defined by

$$2|\mathbf{K}|S_{\mathbf{g}} = -2\mathbf{K}_t.\mathbf{g} - \mathbf{g}^2 \quad (6)$$

and is positive for reciprocal-lattice points inside the Ewald sphere. We define the Laue circle as the intersection of the Ewald sphere with the plane of reciprocal-lattice points excited (the ZOLZ). Here $\mathbf{K}_t(K_x, K_y)$ is a vector drawn from the centre of the Laue circle to the origin of reciprocal space. It is the component of $\mathbf{K}$ in the zero-order Laue zone. The Bragg condition is satisfied if a reciprocal-lattice point falls on the Laue circle. We now consider the geometry of CBED patterns as they appear on film, and the relationship between distances on film and

changes in $\mathbf{K}_t$ and the excitation errors. In practice, distances on the film X are related to reciprocal-space distances g by

$$X = Lg\lambda$$

where L is the electron microscope camera length. For the remainder of this discussion, however, we take $L = 1/\lambda$ for clarity. We consider first the three-beam case, from which other cases may readily be derived. Fig. 1(a) shows this orientation, with, for simplicity, the centres A and B of the CBED discs **g** and **h** at the exact Bragg condition, and therefore on the Laue circle. At A, $S_g = 0$ while, at B, $S_h = 0$. The perpendicular bisectors of OA, AB and OB therefore meet at the centre M of the Laue circle $LS1$ shown. This defines $\mathbf{K}_t$ as the vector from the centre of $LS1$ to the centre O of the (000) disc. The centre of $LS1$ can be identified as the zone axis from the Kikuchi line pattern.

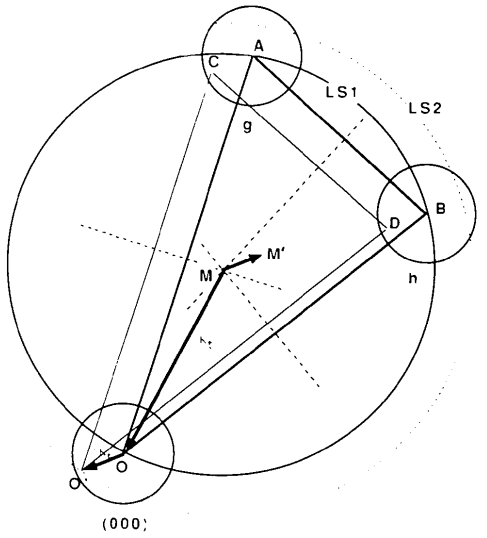

(a)

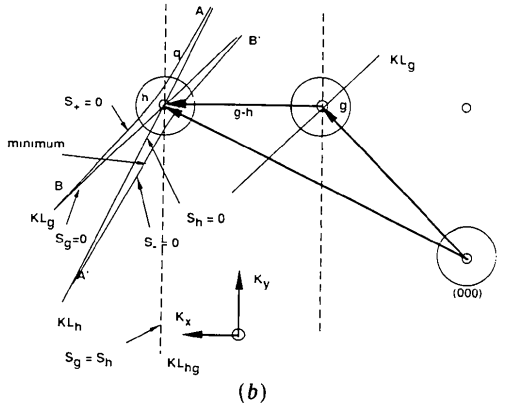

(b)

Fig. 1. (a) Two different 'point' electron diffraction patterns, OAB and $O'CD$, are shown within the CBED discs **0**, **g** and **h**. Their Laue circles are marked $LS1$ and $LS2$, respectively. The zone axis occurs at M, and the Bragg condition is satisfied at A and B. Excitation errors are positive for points C and D which lie inside the Ewald sphere. (b) General form of a three-beam CBED pattern. Kikuchi lines KL_h and KL_g (along which the excitation errors S_h and S_g are zero) are shown. The intensity distribution has extrema on the hyperbolae where $S_+ = 0$ and $S_- = 0$ are shown. The intensity approaches two-beam form at A and A' and fades towards B and B'. For the CdS example, $\mathbf{g} = 41\bar{2}$, $\mathbf{h} = 41\bar{4}$ and $\mathbf{h} - \mathbf{g} = 00\bar{2}$. The position of the minimum is shown for $\Psi = 0$.

We may think of a CBED pattern as a set of *independent* point diffraction patterns, laid side by side. Every point in the incoherently filled illumination aperture gives rise at the sample to an incident plane wave defined by $|\mathbf{K}|$ and $\mathbf{K}_t$. The direct (forward-scattered) beam which results is focused to a point in the (000) CBED disc. There is, however, an inversion symmetry between points on the electron source and the corresponding point in the central disc. Thus, if we imagine Fig. 1(b) to be illuminated from above, the choice of a new source point slightly to the right of O at $-\Delta\mathbf{K}_t$ actually produces a point of intensity at O', where $OO' = \Delta\mathbf{K}_t$ as shown.

The point O' may now be taken as the new origin of a point diffraction pattern, whose conjugate points C and D in the **g** and **h** CBED discs differ by reciprocal-lattice vectors **g** and **h**. If, however, the change in diffraction conditions (rotation of the Ewald sphere) due to $\Delta\mathbf{K}_t$ were referred to the original origin at O, this would move the centre of the Laue circle from M to M'. This displacement is exactly cancelled by the origin shift from O to O' due to the inversion mentioned above. We conclude that the centre of the Laue circle remains fixed in CBED patterns. Laue circles are concentric on experimental CBED patterns. Thus $\mathbf{K}_t$ may be measured from this fixed centre (the zone axis at M in Fig. 1) to any required point in the central disc. This point then defines an incident-beam direction, which makes an angle $\sin^{-1}(K_t/|\mathbf{K}|)$ with the normal to the plane of reciprocal-lattice vectors excited. Conjugate points, differing by reciprocal-lattice vectors, are thereby also defined in all CBED discs, with their associated excitation errors given by (6). In a two-dimensional pattern it is necessary to identify two Bragg conditions to find $\mathbf{K}_t$. This is done using the Kikuchi lines. We may therefore think of the CBED pattern as a function of $\mathbf{K}_t$, which originates in the centre of the triangle OAB shown and extends to a point of interest in the central disc.

Fig. 1(b) shows the general form of the contrast seen in three-beam patterns for a range of incident plane waves. The excitation errors S_g and S_h are zero along the Kikuchi lines KL_g and KL_h respectively in Fig. 1(b). For convenience in this paper we plot all the computed CBED patterns as functions of K_x and K_y.

The mean electron wave vector inside the crystal is

$$|\mathbf{K}|^2 = U_0 + 2m|e|E/h^2 \qquad (7)$$

with E the accelerating voltage.

For crystals with a centre of symmetry all the U_g are real (positive or negative). For this case an exact solution for the γ^i in (5) was obtained at the degeneracy point by Gjønnes & Høier (1971), who derived the following expression for the excitation errors at which the gap $\Delta\gamma$ between two dispersion surface branches is zero:

$$2KS_g = [U_g(U_{g-h}^2 - U_h^2)]/U_h U_{g-h} \quad (8)$$

and

$$2KS_h = [U_h(U_{g-h}^2 - U_g^2)]/U_g U_{g-h}. \quad (9)$$

Solutions for the C_g at the degeneracy point have also been obtained in unpublished work by J. Gjønnes, and by Hurley & Moodie (1980) along lines through the degeneracy point parallel to $S_g = 0$ and $S_h = 0$. The general solution of (5) may also be obtained. This lengthy and complicated expression provides little insight into the optimum choice of experimental conditions. We therefore now first consider two approximations which have proven useful, and then summarize the general features of three-beam patterns. The first of these (due to Bethe) uses plane waves for the asymptotic form of the wave field, while the second (due to Kambe) uses Bloch waves.

3. The second Bethe approximation for non-centrosymmetric crystals and its validity domain

Using a perturbation series, Bethe (1928) has shown how the effects of beams other than those included in the two-beam theory may be incorporated using modified effective potentials U^{eff}. The geometry is shown in Fig. 1(*b*). This corresponds to the case of the $\mathbf{h} = 41\bar{4}$ and $\mathbf{g} = 41\bar{2}$ reflections in the non-centrosymmetric CdS structure to be discussed later. We take a primary (strong) beam **h** and a weaker coupled beam **g**. Fig. 1 illustrates this case if beam **h** is near its Bragg condition along the line AA' or KL_h in Fig. 1(*b*). In this first Bethe approximation, with $U_g \neq U_{-g}$ for acentric crystals, the two-beam dispersion equation becomes

$$\begin{vmatrix} -2K\gamma - U_{11} & U_h^{\text{eff}} \\ U_h^{\text{eff}} & -K\gamma + 2KS_h - U_{22} \end{vmatrix} = 0, \quad (10)$$

where

$$U_h^{\text{eff}} = U_{-h} - U_{12} = U_{-h} - \sum_{g \neq 0,h} (U_{-g}U_{g-h})/2KS_g$$
$$U_h^{\text{eff}} = U_h - U_{21} = U_h - \sum_{g \neq 0,h} (U_g U_{h-g})/2KS_g \quad (11)$$

and

$$U_{11} = \sum_{g \neq 0,h} (U_{-g}U_g)/2KS_g$$
$$U_{22} = \sum_{g \neq 0,h} (U_{h-g}U_{g-h})/WKS_g. \quad (12)$$

The expression for the intensity in a many-beam CBED pattern in a non-centrosymmetric crystal can then be put into two-beam form by defining an effective eigenvalue

$$2K\gamma^{\text{eff}} = 2K\gamma + U_{11}$$

and an effective excitation error

$$2KS_h^{\text{eff}} = 2KS_h + U_{11} - U_{22}. \quad (13)$$

We then obtain a dispersion matrix

$$\begin{vmatrix} -2K\gamma^{\text{eff}} & U_h^{\text{eff}} \\ U_h^{\text{eff}} & -2K\gamma^{\text{eff}} + 2KS_h^{\text{eff}} \end{vmatrix} = 0. \quad (14)$$

The two-beam expression for the diffracted intensity is then

$$I_h = [U_h^{\text{eff}} U_h^{\text{eff}} \sin^2(\pi t \Delta\gamma^{\text{eff}})]/K^2(\Delta\gamma^{\text{eff}})^2 \quad (15)$$

where $\Delta\gamma$ is the difference in the roots of (10). For the particular case of three beams this is given by

$$\begin{aligned}(2K\Delta\gamma^{\text{eff}})^2 &= [2KS_h + (|U_g|^2 - |U_{h-g}|^2)/2KS_g]^2 \\ &\quad + 4|U_h|^2\left[1 - 2\frac{|U_{-g}||U_{h-g}|}{|U_h|2KS_g}\cos\Psi \right. \\ &\quad \left. + \frac{|U_g|^2|U_{g-h}|^2}{|U_h|^2(2KS_g)^2}\right] \\ &= T_1 + T_2. \end{aligned} \quad (16)$$

The effective structure factor is given by

$$\begin{aligned} U_h^{\text{eff}} U_h^{\text{eff}} &= |U_h|^2 - 2\frac{|U_h||U_{-g}||U_{g-h}|}{2KS_g}\cos\Psi \\ &\quad + \frac{|U_g|^2|U_{g-h}|^2}{(2KS_g)^2} \\ &= |U_h|^2\left[\left(1 - \frac{|U_{-g}||U_{g-h}|}{2KS_g|U_h|}\cos\Psi\right)^2 \right. \\ &\quad \left. + \left|\frac{U_g U_{g-h}}{U_h 2KS_g}\sin\Psi\right|^2\right]. \end{aligned} \quad (17)$$

Here the three-phase structure invariant is defined as

$$\Psi = \varphi_h + \varphi_{-g} + \varphi_{g-h} \quad (18)$$

which is independent of the choice of origin in the crystal (the vectors must form a closed loop). φ_h is the phase of U_h.

The important approximations of this theory are that, for the two Bloch waves which dominate the (**0**, **h**) two-beam interaction, $|C_g| \ll 1$. We also require that $|\gamma| \ll S_g$. It is readily shown that these conditions require that

$$|S_g| \gg |U_{\max}|/2K \quad (19)$$

and

$$|S_h| \ll |S_g|, \quad (20)$$

where $U_{\max}$ is the largest structure factor. In the Bethe approximation, plane waves are used as the

asymptotic form of the wave field. In Kambe's method, Bloch waves are used for the **g**–**h** interaction, and a plane wave for the direct beam, as asymptotic forms.

Fig. 2(*a*) shows the domain of validity of this approximation as it appears on a convergent-beam pattern.

4. Kambe's strong-coupling approximation

Solutions to (5) have been obtained by Kambe (1957) for the case where beams **g** and **h** are strongly coupled, *i.e.*

$$|U_{gh}| = |U_{g-h}| \gg |U_g| \text{ or } |U_h|. \tag{21}$$

We now derive these solutions in standard notation and discuss their domain of validity for the non-centrosymmetric case.

First, take $U_g = U_h = 0$ so that (5) becomes

$$\begin{aligned} -2K\gamma C_0 &= 0 \\ 2K(S_g - \gamma)C_g + U_{gh}C_h &= 0 \\ U_{hg}C_g + 2K(S_h - \gamma)C_h &= 0. \end{aligned} \tag{22}$$

This gives

$$\begin{aligned} \gamma^1 &= 0 \\ 2\gamma^{2,3} &= \{S_g + S_h \pm [(S_g - S_h)^2 + |U_{gh}/K|^2]\}^{1/2} \end{aligned} \tag{23}$$

and

$$C_0^{(1)} = 1, \quad C_g^{(1)} = C_h^{(1)} = 0 \tag{24}$$

$$C_0^{(2)} = 0, \quad C_g^{(2)} = \cos(\beta/2)\exp(i\varphi_{gh}),$$

$$C_h^{(2)} = \sin(\beta/2) \tag{25}$$

$$C_0^{(3)} = 0, \quad C_g^{(3)} = -\sin(\beta/2),$$

$$C_h^{(3)} = \cos(\beta/2)\exp(-i\varphi_{gh}) \tag{26}$$

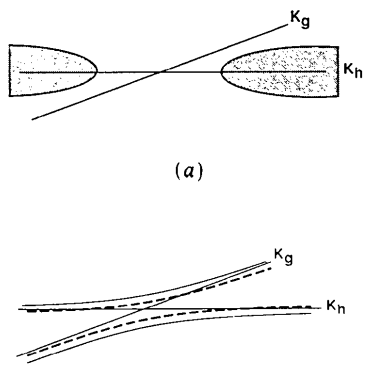

Fig. 2. (*a*) The shaded regions represent the validity domains for the second Bethe approximation in three-beam patterns [see equations (19) and (20)]. (*b*) The Kambe 'strong coupling' approximation holds above and below the dashed lines shown.

Here φ_{gh} is the phase of U_{gh} and $\cot\beta = (S_g - S_h)K/|U_{gh}|$. These results provide the asymptotic solutions for $U_g \neq 0$ and $U_h \neq 0$, as can be seen from a study of the three-beam dispersion surface geometry. We therefore use the Bloch waves defined by (24)–(26) as basis functions for the solution of (5). The wave field inside the crystal is written as

$$\psi(\mathbf{r}) = (C_0 + C_+\psi_+ + C_-\psi_-)\exp(2\pi i\mathbf{k}.\mathbf{r}) \tag{27}$$

with $\mathbf{k} = \mathbf{K} + \gamma\mathbf{z}$. Here $\mathbf{z}$ is into the crystal and positive eigenvalues denote dispersion surfaces above the sphere of radius $|\mathbf{K}|$.

$$\begin{aligned} \psi_+ &= \cos(\beta/2)\exp(i\varphi_{gh}) - \exp(2\pi i\mathbf{g}.\mathbf{r}) \\ &\quad + \sin(\beta/2)\exp(2\pi i\mathbf{h}.\mathbf{r}) \end{aligned} \tag{28}$$

$$\begin{aligned} \psi_- &= -\sin(\beta/2)\exp(2\pi i\mathbf{g}.\mathbf{r}) \\ &\quad + \cos(\beta/2)\exp(-i\varphi_{gh})\exp(2\pi i\mathbf{h}.\mathbf{r}). \end{aligned} \tag{29}$$

Regrouping terms in unity, $\exp(2\pi i\mathbf{g}.\mathbf{r})$ and $\exp(2\pi i\mathbf{h}.\mathbf{r})$, we find the following relations between the eigenvector elements:

$$\begin{pmatrix} C_0 \\ C_g \\ C_h \end{pmatrix} = \begin{pmatrix} 1 & 0 & 0 \\ 0 & \exp(i\varphi_{gh})\cos(\beta/2) & \sin(\beta/2) \\ 0 & -\sin(\beta/2) & \exp(-i\varphi_{gh})\cos(\beta/2) \end{pmatrix} \begin{pmatrix} C_0 \\ C_+ \\ C_- \end{pmatrix}. \tag{30}$$

Using (30) in (5) we obtain after some manipulation

$$\begin{pmatrix} 0 & U_+^* & U_-^* \\ U_+ & 2KS_+ & 0 \\ U_- & 0 & 2KS_- \end{pmatrix} \begin{pmatrix} C_0 \\ C_+ \\ C_- \end{pmatrix} = 2K\gamma \begin{pmatrix} C_0 \\ C_+ \\ C_- \end{pmatrix}. \tag{31}$$

Here

$$U_+ = U_g\cos(\beta/2)\exp(-i\varphi_{gh}) + U_h\sin(\beta/2) \tag{32}$$

$$U_- = -U_g\sin(\beta/2) + U_h\cos(\beta/2)\exp(i\varphi_{gh}) \tag{33}$$

$$S_+ = \tfrac{1}{2}\{S_g + S_h + [|U_{gh}/K|^2 + (S_g - S_h)^2]^{1/2}\} \tag{34}$$

$$S_- = \tfrac{1}{2}\{S_g + S_h - [|U_{gh}/K|^2 + (S_g - S_h)^2]^{1/2}\}. \tag{35}$$

Setting $S_+ = 0$ or $S_- = 0$ defines the hyperbola AB or $A'B'$ on which the intensity is maximum.

Despite the simplification of equation (31), a simple analytical solution is still not possible. We note, however, that in the region where S_+ is small the minimum value of $|S_-|$ is $|U_{gh}|/K$. From (32) and (33) the largest value of U_+ and U_- is $|U_g| + |U_h|$. Hence we have

$$|2KS_-| \gg |U_+| \text{ or } |U_-| \tag{36}$$

and

$$|2KS_-| \gg 2K|S_+|. \tag{37}$$

Solutions for this region can then be found, since, by a similar argument to that used in §3 [equations (19),

(20)], we take $C_- = 0$. Then (31) becomes

$$\begin{pmatrix} 0 & U_+^* \\ U_+ & 2KS_+ \end{pmatrix}\begin{pmatrix} C_0 \\ C_+ \end{pmatrix} = 2K\gamma\begin{pmatrix} C_0 \\ C_+ \end{pmatrix}, \tag{38}$$

which has the roots

$$\gamma^{1,2} = \tfrac{1}{2}\{S_+ \pm [S_+^2 + |U_+/K|^2]^{1/2}\}. \tag{39}$$

Let $\cot\alpha = S_+K/|U_+|$. Then

$$C_0^{(1)} = \cos(\alpha/2)\exp(-i\varphi_+)$$

and

$$C_0^{(2)} = \sin(\alpha/2)\exp(-i\varphi_+)$$

$$C_+^1 = -\sin(\alpha/2) \quad \text{and} \quad C_+^2 = \cos(\alpha/2).$$

Here

$$\varphi_+ = \varphi_g - \varphi_{g-h} + \theta$$

and

$$\tan\theta = \tan(\beta/2)|U_h/U_g|\sin\psi \times [1 + \tan|\beta/2||U_h/U_g|\cos\psi]^{-1}. \tag{40}$$

From (30), we have then

$$C_g \simeq C_+\exp(i\varphi_{gh})\cos(\beta/2)$$

and

$$C_h \simeq -C_+\sin(\beta/2). \tag{41}$$

Using the above results and equation (3), we find that near the line AB in Fig. 1(b) where S_+ is small and (36) and (37) are satisfied,

$$I_g = \Phi_g\Phi_g^* = (1+|S_+K/U_+|^2)^{-1} \times \cos^2(\beta/2)\sin^2[\pi t(S_+^2+|U_+/K|^2)^{1/2}] \tag{42}$$

$$I_h = \Phi_h\Phi_h^* = (1+|S_+K/U_+|^2)^{-1} \times \sin^2(\beta/2)\sin^2[\pi t(S_+^2+|U_+/K|^2)^{1/2}]. \tag{43}$$

Similarly, near the line $A'B'$ in Fig. 1(b) where S_- is small,

$$I_g = \Phi_g\Phi_g^* = (1+|S_-K/U_-|^2)^{-1} \times \sin^2(\beta/2)\sin^2[\pi t(S_-^2+|U_-/K|^2)^{1/2}] \tag{44}$$

$$I_h = \Phi_h\Phi_h^* = (1+|S_-K/U_-|^2)^{-1} \times \cos^2(\beta/2)\sin^2[\pi t(S_-^2+|U_-/K|^2)^{1/2}]. \tag{45}$$

Fig. (2b) shows the region in which these solutions hold, and should be compared with the validity domain of the Bethe potential solution shown in Fig. 2(a).

Of the quantities involved in these intensity expressions, only $|U_+|^2$ and $|U_-|^2$ depend on structure-factor phases. From (32) and (33) we have

$$|U_+|^2 = |U_h|^2\sin^2(\beta/2) \times \{[1+|U_g/U_h|^2\cot(\beta/2)\cos\Psi]^2 + |U_g/U_h|^2\cot^2(\beta/2)\sin^2\Psi\} \tag{46}$$

$$|U_-|^2 = |U_h|^2\cos^2(\beta/2) \times \{[1-|U_g/U_h|^2\tan(\beta/2)\cos\Psi]^2 + |U_g/U_h|^2\tan^2(\beta/2)\sin^2\Psi\}, \tag{47}$$

with Ψ again the three-phase invariant [(18)].

We now show that these results agree with those of the Bethe approximation for small $S_+ = 0$ (on the line AB) or small $S_- = 0$ (on the line $A'B'$), and $|S_g| \gg |S_h|$ or $|U_{g-h}/K|$ (Bethe approximation). For small S_+

$$\cot(\beta/2) \simeq -|U_{gh}|/2KS_g. \tag{48}$$

Here $\sin(\beta/2) \simeq 1$, while $\cos(\beta/2) \simeq 0$. Hence (46) and (47) become, in this region,

$$|U_+|^2 = |U_h|^2\left[\left(1 - \frac{|U_{-g}||U_{g-h}|}{2KS_g|U_h|}\cos\Psi\right)^2 + \left|\frac{U_gU_{g-h}}{U_h 2KS_g}\sin\Psi\right|\right]. \tag{49}$$

Similarly, near $S_- = 0$ where $|S_g| \gg |S_h|$ or $|U_{g-h}/K|$,

$$\tan(\beta/2) \simeq |U_{gh}|/2KS_h. \tag{50}$$

Here $\sin(\beta/2) \simeq 0$ with $\cos(\beta/2) \simeq 1$. Then

$$|U_-|^2 = |U_g|^2\left[\left(1 - \frac{|U_{-h}||U_{g-h}|}{2KS_g|U_g|}\cos\Psi\right) + \left|\frac{U_hU_{g-h}}{2KS_gU_g}\sin\Psi\right|^2\right]. \tag{51}$$

5. General features of three-beam patterns in non-centrosymmetric crystals

The results of the previous sections may be used to draw some qualitative and quantitative conclusions about the form of three-beam patterns from non-centrosymmetric crystals. Bands of maximum intensity might be expected on the lines AB and $A'B'$ in Fig. 1(b), along which the effective excitation errors S_+ or S_- of three-beam theory are zero, respectively. In fact, owing to dynamical effects, the intensity is modulated as shown schematically in the figure, and a gap appears near the crossing of these lines. For certain thicknesses (*e.g.* $t < K/2U_{+/-}$), equations (34), (35), (42) and (43) give the locus of the two bands as $S_+ = 0$ and $S_- = 0$. The distance between these bands measured along the line $S_g = S_h$ shown may be obtained from the same equations as $|U_{g-h}|/K$.

Equations (42) and (43) also show that, owing to the factors $\cos^2(\beta/2)$ and $\sin^2(\beta/2)$, the intensity of beam **h** falls off as $|S_g|$ becomes large, as observed experimentally (see Figs. 3 and 6).

These general trends are demonstrated by the two-dimensional three-beam calculations shown in Figs. 3 for GaAs.

For $t < K/2|U_{+/-}|$ the intensity in the CBED pattern is proportional to the effective potential $U_{+/-}$, which has either a maximum on $A'B'$ and a minimum on AB, or the converse, depending on whether $\cos\Psi$ is less than or greater than zero. [The minimum in Fig. 1(b) is drawn for $\Psi = 0$.] From (42) and (43) the positions of these maxima and minima are given by

$$S_h \simeq (|U_{gh}|/4K\cos\Psi)\{|U_h|/|U_g| - |U_g|/|U_h| \pm [(|U_g|/|U_h| - |U_h|/|U_g|)^2 + 4\cos^2\Psi]^{1/2}\}. \quad (52)$$

Along the hyperbolae the incident beam is constrained to move such that

$$S_g = |U_{gh}|^2/4K^2 S_h. \quad (53)$$

The upper sign in (52) gives the maximum. In a centrosymmetric crystal with $\Psi = 0$ the minimum is on the upper band $A'B'$ at

$$S_h \simeq |U_{gh}||U_h|/2K|U_g| \quad (54)$$

and

$$S_g \simeq |U_{gh}||U_g|/2K|U_h|. \quad (55)$$

The maximum occurs on the band AB where

$$S_h \simeq -|U_{gh}||U_g|/2K|U_h| \quad (56)$$

and

$$S_g \simeq -|U_{gh}||U_h|/2K|U_g|. \quad (57)$$

The signs of all these excitation errors are reversed for $\Psi = \pi$.

These results [(54) and (55)] may be compared with those of (8) and (9) from § 2, which were obtained from the full solution. We see that the above approximate expressions for the position of the degeneracy are justified if $|U_{g-h}| \gg |U_g|$ or $|U_h|$.

It has been suggested that the distance between the maximum and minimum intensity may be used to measure the three-phase invariant (Bird, James & Preston, 1987). Within the Kambe approximation this

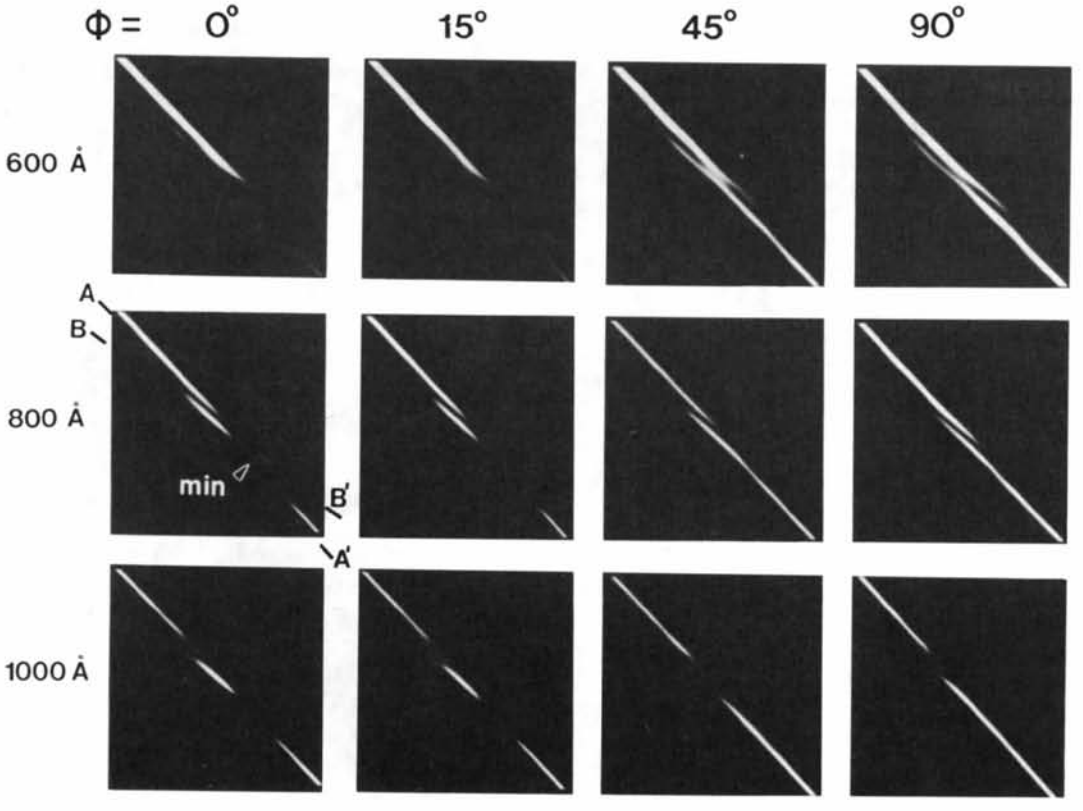

Fig. 3. The variation of three-beam patterns with thickness and phase. Each column corresponds to the same value of the three-phase invariant, while the thickness changes with each row. These are three-beam dynamical calculations for the $\bar{1}7\bar{5}$ reflection in GaAs at 120 kV. The other reflections are 000 and $\bar{2}6\bar{4}$. The values $U(\bar{1}7\bar{5}) = 0{\cdot}0139$, $U(\bar{2}6\bar{4}) = 0{\cdot}0250$ and $U(11\bar{1}) = 0{\cdot}0512$ were used. The figure is related by a vertical mirror plane of reflection to Fig. 1(b).

distance is, from (52),

$$d = S_{\mathbf{h}}^{\max} - S_{\mathbf{h}}^{\min}$$
$$= (|U_{\mathbf{gh}}|/2K\cos\Psi) \times [(|U_{\mathbf{g}}|/|U_{\mathbf{h}}| - |U_{\mathbf{h}}|/|U_{\mathbf{g}}|)^2 + 4\cos^2\Psi]^{1/2}. \quad (58)$$

Distances measured from electron micrographs must, however, be rescaled according to (6).

The three-phase invariant can therefore be found using

$$|\cos\Psi| = (|U_{\mathbf{g}}|/|U_{\mathbf{h}}| - |U_{\mathbf{h}}|/|U_{\mathbf{g}}|) \times [2(d^2K^2/|U_{\mathbf{gh}}|^2 - 1)^{1/2}]^{-1}. \quad (59)$$

The positions of the maxima and minima immediately indicate the sign of $\cos\Psi$, which is positive as drawn in Fig. 1(*b*). We note that the positions of the maximum and minimum are not symmetrical in $S_{\mathbf{h}}$ and $S_{\mathbf{g}}$. The earlier approximate result (Bird, James & Preston, 1987) for d was based on the first terms of the Born series in the approximation of weak coupling. This result predicts multiple maxima and minima, not present in the above dynamical treatment or in experimental results.

To summarize, the following intensity variations will be observed in three-beam patterns from *centrosymmetric* crystals where $\Psi = 0$ or π. For $\Psi = 0$ the elastic intensity along $A'B'$ falls to zero at the degeneracy point shown in Fig. 1(*b*) (labelled 'minimum'). For $\Psi = \pi$ the zero occurs for opposite signs of the excitation errors, *i.e.* near q. For a *non-centrosymmetric* crystal this zero intensity becomes a minimum of intensity. For Kikuchi lines, this occurs when $\Delta\gamma$ (the dispersion surface gap) is a minimum since the band of intensity along AB is a projection of the position and width of the dispersion surface gap (Gjønnes & Høier, 1971). The results of § 3 on the Bethe approximation can also be used to obtain an expression for the position of the minimum. Setting $T_1 = 0$ in (16) and using the result in the minimum value of T_2 with respect to $S_{\mathbf{g}}$ gives

$$2KS_{\mathbf{g}} \simeq |U_{\mathbf{g}}||U_{\mathbf{g-h}}|/|U_{\mathbf{h}}|\cos\Psi$$

and

$$2KS_{\mathbf{h}} \simeq [|U_{\mathbf{h}}|(|U_{\mathbf{g-h}}|^2 - |U_{\mathbf{g}}|^2)/|U_{\mathbf{g}}||U_{\mathbf{g-h}}|]\cos\Psi \quad (60)$$

for the position at which the minimum occurs. For a centrosymmetric crystal with $\Psi = 0$ and $|U_{\mathbf{g-h}}| \gg |U_{\mathbf{g}}|$ or $|U_{\mathbf{h}}|$ (strong coupling), (60) reduces to (55). The condition $S_+ = S_- = 0$ defines the curves AB and $A'B'$ in terms of excitation errors, within the shaded area of Fig. 2(*a*). If the structure-factor amplitudes are known, (60) also allows the determination of the three-phase invariant Ψ. A determination of several linked phase invariants provides a relationship between complex structure factors, and so may be used to assist in structure analysis. In other cases two of the three phases may be known or zero. For these excitation errors [(60)] the minimum dispersion surface gap width, in the Bethe approximation, is

$$\Delta(2K\gamma) = 2|U_{\mathbf{h}}\sin\Psi|. \quad (61)$$

The intensity profiles (as a function of $S_{\mathbf{h}}$) at other positions may be obtained from (15) along lines parallel to $KL_{\mathbf{g}}$, for which $S_{\mathbf{g}}$ is constant. We note in passing that for the study of the inelastic scattering responsible for Kikuchi lines, the thickness-dependent term in equations (15), (42), (43), (44) and (45) is neglected in the independent-Bloch-wave approximation. This approximation forms the basis of the intersecting-Kikuchi-line method.

6. Absorption in three-beam theory for non-centrosymmetric crystals

For reasons of clarity and analytic simplicity, the preceding discussion has not considered the effects of absorption on the three-beam theory. As in the two-beam dynamical theory, absorption terms can be included to take account of the depletion of the elastic wave field by inelastic processes. Experimentally, we observe that the intensity on the upper branch of the hyperbola is always slightly less than that on the lower branch, an effect which we now show is due to absorption.

In first-order perturbation theory, the corrections to the eigenvalues of the dispersion matrix are found to be

$$\gamma'^i = \gamma^i + iq^i$$

where

$$2Kq^i = \sum_{\mathbf{h}} U'_{\mathbf{g-h}} C_{\mathbf{h}}^i C_{\mathbf{g}}^{i*} = Q^i.$$

Using the unperturbed eigenvectors of (40) and (41) we find the absorption factors to be as follows. For the upper branch (S_+ small),

$$Q^1 = -|U'_0| + |U'_{\mathbf{g}}|\sin\alpha\cos(\beta/2)\cos\theta + |U'_{\mathbf{h}}|\cos(\Psi-\theta)\sin\alpha\sin(\beta/2) - |U'_{\mathbf{g-h}}|\sin\beta\sin^2(\alpha/2)$$
$$Q^2 = -|U'_0| - |U'_{\mathbf{g}}|\sin\alpha\cos(\beta/2)\cos\theta - |U'_{\mathbf{h}}|\cos(\Psi-\theta)\sin\alpha\sin(\beta/2) - |U'_{\mathbf{g-h}}|\sin\beta\sin^2(\alpha/2)$$

while, on the lower branch (S_- small),

$$Q^1 = -|U'_0| - |U'_{\mathbf{g}}|\sin\alpha'\cos(\beta/2)\cos\theta' + |U'_{\mathbf{h}}|\cos(\Psi-\theta')\sin\alpha'\sin(\beta/2) + |U'_{\mathbf{g-h}}|\sin\beta\sin^2(\alpha'/2)$$
$$Q^2 = -|U'_0| + |U'_{\mathbf{g}}|\sin\alpha'\cos(\beta/2)\cos\theta' - |U'_{\mathbf{h}}|\cos(\Psi-\theta')\sin\alpha'\sin(\beta/2) + |U'_{\mathbf{g-h}}|\sin\beta\sin^2(\alpha'/2).$$

Here θ was defined in (40), while $\cot\alpha' = S_- K/|U_-|$ and

$$\tan\theta' = \frac{-\cot(\beta/2)|U_h U_g|\sin\Psi}{1-\cot(\beta/2)|U_h/U_g|\cot\Psi}.$$

The effect of absorption is to introduce terms $\exp(\pi t Q^i/K)$ into the expression for a particular beam amplitude [equation (4)]. Thus the two negative terms in $|U_{g-h}|$ in the expression for Q^i on the upper branch leads to a decrease of intensity. Here $\sin(\beta/2)$ is always positive. On the lower branch similar positive terms lead to an increased intensity, as observed experimentally.

7. Experimental application to CdS

For the non-centrosymmetric CdS structure, the intensity along the hyperbolae may, within the Kambe approximation, be expressed using (34), (43), (45), (46) and (47) as

$$I_h = \frac{(2KS_g)^2}{|U_{h-g}|^2+(2KS_g)^2}\sin^2(\pi t|U_h^{\rm eff}|/K), \quad (62)$$

with

$$|U_h^{\rm eff}|^2 = |U_h|^2\frac{(2KS_g)^2}{|U_{h-g}|^2+(2KS_g)^2} \times\left[\left(1-\frac{|U_g||U_{h-g}|}{2KS_g|U_h|}\cos\Psi\right)^2 + \left(\frac{|U_g||U_{h-g}|}{2KS_g|U_h|}\sin\Psi\right)^2\right]. \quad (63)$$

With (53), equations (62) and (63) can also be expressed entirely in terms of S_h.

In (62), S_g is negative on the upper hyperbola AB and positive on the lower. The prefactor in (62) is independent of phase, and accounts for a slow reduction in the intensity of I_h near B and B' where $S_g = 0$. The intensity is greatest near A and A'. From (62) we see that for thicknesses $t = (n+1/4)\,\xi_h$ the intensity is most sensitive to changes in $U_h^{\rm eff}$, and hence to Ψ. Here the slope of the *Pendellösung* curve is also steepest. The intensity along the hyperbolae has either a maximum on the upper hyperbola ($S_g < 0$) and a minimum on the lower ($S_g > 0$), or the converse, depending on whether $\cos\Psi$ is greater or less than zero. The variation of the effective potential $U_h^{\rm eff}$ with excitation error for several values of the three-phase invariant is shown in Fig. 4. Values of U_g have been taken from *International Tables for X-ray Crystallography* (1974). The structure factors for CdS are given by

$$F_{hkl} = [f_{\rm Cd} + f_{\rm S}\exp(2\pi i l u)][\exp 2\pi i(2h/3+k/3) + \exp 2\pi i(h/3+2k/3+l/2)]. \quad (64)$$

Here $k-h = 3n$ (n an integer) in the $[\bar{1}40]$ ZOLZ.

Experimentally it is difficult to measure the electron intensity along the hyperbolae. Therefore we have taken line scans parallel to KL_{hg} in Fig. 1(b) at several places cutting both hyperbolae, and compared the results with full many-beam calculations. In this way a value of Ψ may be refined. It is clear that the most sensitive region for such a scan is at the minimum shown in Fig. 4.

Crushed samples of single-crystal hexagonal CdS were examined in a Philips EM400T electron microscope at room temperature. CBED patterns were obtained using a probe size of about 100 nm, and recorded on film. The processed negatives were read into a VAX 750 computer using a charge-coupled device (CCD) camera to minimize field distortion. Allowance was made for the logarithmic response of the film to light, but linear response to electrons. This method is quick and convenient and takes advantage of the large storage capacity of film. However, the resulting patterns include an inelastic background. For the systematic orientation, where one-dimensional data are used, we have found an energy-loss spectrometer useful for recording the elastic intensity. The pattern is scanned, under computer control, over the spectrometer entrance slit. We have also developed a liquid-nitrogen-cooled yttrium aluminium garnet (YAG)-CCD detection system with large dynamic range for parallel detection on the electron microscope (Spence & Zuo, 1988). Using this system, which reads two-dimensional data directly into a computer, we expect increased accuracy in phase determination because of its larger dynamic range (14 bits).

The subtraction of the background due to inelastic scattering presents special problems in two-dimensional patterns. In the present work the background was subtracted as follows. A point diffraction pattern taken from the same region used for analysis was recorded under identical conditions, and read into the computer. The resulting peaks were then fitted to the Lorentzian function which describes small-angle scattering by electronic excitations, plas-

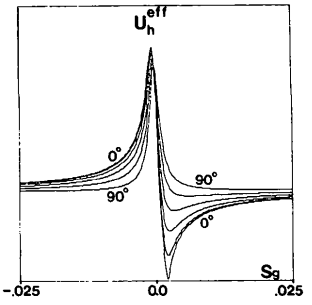

Fig. 4. Variation of the effective potential $U_h^{\rm eff}$ (Kambe) with excitation error for equal increments in the phase invariant between 0 and 90°. This quantity is related to the intensity in three-beam CBED patterns along AB ($S_g < 0$) and $B'A'$ ($S_g > 0$) (see Fig. 1b). Asymptotes are $|U_h|$.

mons and some phonons. This was convoluted with a top-hat function representing the incident-beam divergence (for the point pattern), and the result convoluted with the results of the many-beam calculations. This procedure avoids the noise-amplification problems well known to be associated with deconvolution.

Fig. 5 shows the pattern used for analysis, while Fig. 6 shows an enlarged view of the $(41\bar{4})$ CBED disc, and the positions of two line scans XX' and YY' taken across it. The results of the scans are shown in Fig. 7. The scan lines run parallel to KL_{hg} in Fig. 1(b). The gap in the upper hyperbola in Fig. 6 is due to an additional interaction (the $00\bar{6}$), which is fully included in the many-beam calculations. The horizontal band of intensity which runs across the bottom of the image is modulated by perturbations due to the $00h$ systematic line on the left, and to the 410 reflection on the right. This band produces the unimportant smaller peaks near X and Y in Fig. 7. The two main peaks in Fig. 6 are identified by the arrows in Fig. 7. These peaks lie on the locus of the three-beam hyperbola, which is most sensitive to phase. The beam direction (K_x, K_y) was accurately measured along XX' and YY' for use in the computer calculations.

The many-beam Bloch-wave calculations for the intensity along XX' and YY' in Fig. 6 depend on the following parameters, which were found as follows: (1) The accelerating voltage was determined from an analysis of HOLZ line positions. (2) Absorption

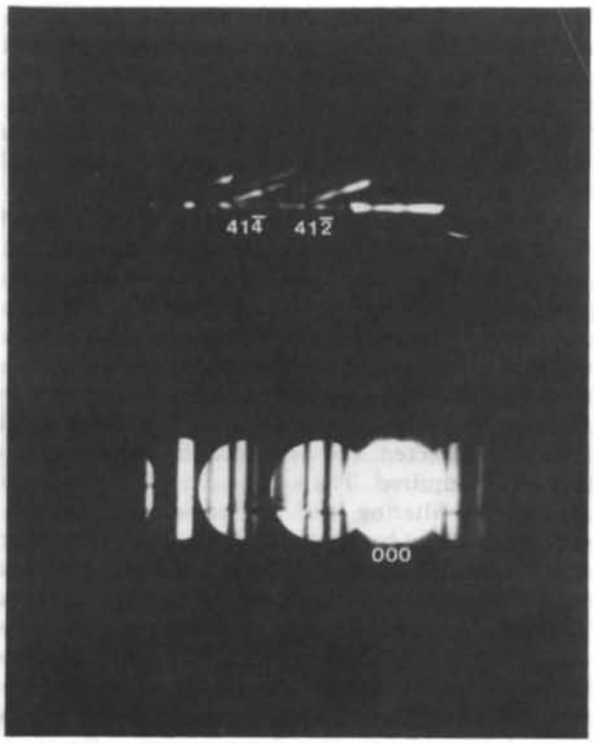

Fig. 5. Small-camera-length view of the CBED pattern used to determine a three-phase invariant in CdS. The three strong beams are indexed. All others carrying appreciable intensity are also included in the calculations shown in Fig. 7.

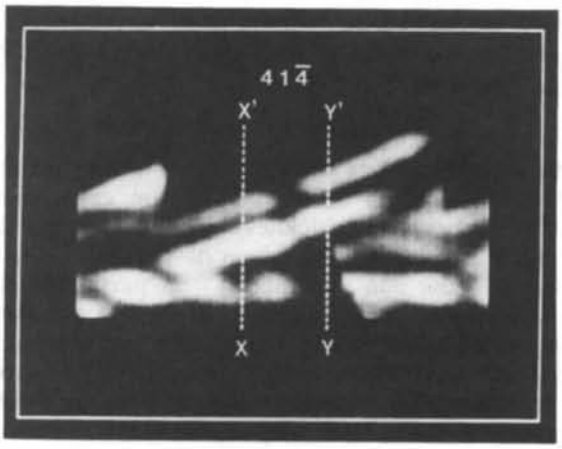

Fig. 6. Enlarged view of the 41$\bar{4}$ CBED disc used for analysis. The lines indicate the positions of the intensity profiles shown in Fig. 7. Other features are discussed in the text.

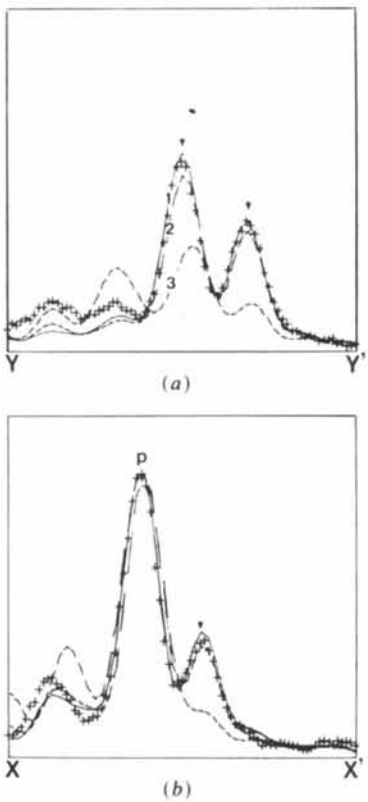

Fig. 7. (a) Comparison of experimental intensity (crosses) and the results of 15-beam dynamical calculations for the intensity along the line YY' indicated in Fig. 6 for three values of the three-phase invariant. These are 49·6° (curve 1), 59·6° (curve 2) and 89·6° (curve 3). The best fit is obtained for $\Psi = 49{\cdot}6°$. Arrows indicate peaks dominated by the three-beam interaction sensitive to phase. (b) Similar to (a) but for the line XX' in Fig. 6. In this region the intensity is less sensitive to phase. The data were normalized at P.

coefficients for reflection **g** were obtained by matching the asymmetry in the 000 disc against calculations with reflection **g** at the Bragg angle. We find $U'(00\bar{2})/U(002) = 0{\cdot}08 \pm 0{\cdot}005$ and $U'(00\bar{6})/(006) = 0{\cdot}1$. This allows a parametric fit to be made to the absorption potential of the form (Voss, Lehmpfuhl & Smith, 1980)

$$U'_g/U_g = -0{\cdot}13g - 0{\cdot}03g^2. \qquad (65)$$

This expression was used to obtain values for the other U'_g required in the many-beam calculation. (3) The specimen thickness was found to be 86·5 (5) nm from a comparison of 32-beam calculations with the $00h$ systematics - in particular, the outer thickness-sensitive fringes of the $00\bar{4}$ disc were used. Data were read from film into the computer, again using a CCD camera. (4) Debye–Waller factors were taken from recent accurate X-ray work (Stevenson, Milanko & Barnea, 1984).

Figs. 7(*a*) and (*b*) show a comparison of the experimental intensity (crosses) and the results of 15-beam calculations for two cuts across the hyperbolae. The second cut at XX' where the data are relatively insensitive to phase was used for normalization. The arrows indicate the two peaks dominated by the three-beam interaction, which are sensitive to phase. Calculations are shown for three values of the three-phase invariant. A statistically significant difference between theory and experiment resulted from a 5° change in phase, which we take to be the error. Unfortunately the most sensitive region could not be used, since it is disturbed by the 410 interaction, which causes the gap in Fig. 6. The calculations solve the time-independent Schrödinger equation by the eigenvalue (Bloch-wave) method for a 120 kV electron traversing a thin slab of parallel-sided non-centrosymmetric crystal which may be inclined to the beam. Absorption is included. The renormalized eigenvector method is used (Lewis, Villagrana & Metherell, 1978), and all HOLZ reflections included. The Fortran source code has been published (Zuo, Gjønnes & Spence, 1988).

From Fig. 7 we find that the sum of the phases of the $4\bar{1}4$, $41\bar{2}$ and $00\bar{2}$ electron structure factors U_g (dimensions length^{-2}) in hexagonal CdS is $49{\cdot}6 \pm 5°$. If it is assumed that two of these phases were known exactly, then the error in the third $00\bar{2}$ X-ray structure-factor phase would be $\pm 0{\cdot}75°$.

8. Discussion and concluding remarks

We may conclude that: (1) the three-beam non-systematic CBED geometry provides a useful general method for obtaining values of the three-phase structure invariants. Because in this case we were not able to use the most sensitive region of the CBED pattern in this work, we are unable to assess its accuracy fully. (2) With the assumption that accurate Debye–Waller factors are available, the most important limitation to the accuracy of this method is the uncertainty in the estimate of background due to inelastic scattering, which has a two-dimensional variation, and the possibility of accidental reflections obscuring the sensitive region of the pattern.

Similar information may be obtained from electron channelling patterns. These phase invariants may be used as starting values for structure refinement by other methods, for which they provide useful constraints.

Our most recent research (Zuo, Spence & Høier, 1989) also suggests that, in particular cases, a variant of the critical voltage method in the systematic geometry may also be used for accurate phase measurements. This in turn would also allow the refinement of atom positions and measurements of bonding charge distributions. For CdS, which is a one-parameter structure, it appears possible to determine the phase of a two-phase (electron) invariant by this method with an accuracy of about 0·9° if the position parameter is assumed known. The error in the corresponding X-ray phase is 0·069°. Alternatively, if an ionicity is assumed, it would be possible to determine the dimensionless atomic position parameter to within about 0·0005. These effects might be disentangled from a series of patterns emphasizing different orders.

The Bethe and Kambe approximations are seen to be well suited for interpretive purposes, and for the analysis of the various parameter dependences. It should be noted, however, that the expressions are not able to distinguish between positive and negative phase angles. This means that they are well behaved in the centrosymmetric case, but should be used with care in the non-centrosymmetric case.

In comparing some of the various methods which have been proposed for electron crystallography, our experience suggests that the three-beam non-systematic method is the most generally useful for non-centrosymmetric crystals requiring phase determination. However, it requires the handling of two-dimensional data sets, and is limited in accuracy by the two-dimensional nature of the background which must be subtracted. For more accurate work, energy filtering is required. The systematic geometry facilitates energy filtering, and any remaining (phonon) background may be estimated from scans taken outside the CBED discs, since this background is also one-dimensional. It is therefore the preferred method for centrosymmetric crystals, in which phases are not required. It may also be used for very accurate phase determination in acentric crystals in many cases, if equation (4) of Zuo, Spence & Høier (1989) can be satisfied. This requires that the minimum in the Bethe effective potential be positioned by choice of accelerating voltage close to the Bragg condition for a second-order reflection. This may not always be

possible, but provides a very simple and accurate method if it is. The systematic geometry also has the advantage of providing many independent structure factors, unlike the more accurate critical voltage method, which provides only a relationship between structure factors. The intersecting-Kikuchi-line method can also provide useful approximate values of structure factors, and is by far the easiest to apply since it relies on distance measurements taken from film, rather than intensity measurements.

This work was carried out during the sabbatical visit of one of us (RH, supported by a grant from NTNF, Norway) to the NSF National Center for High Resolution Electron Microscopy at Arizona State University. It was supported by NSF grant DMR88-13879. We are grateful to Drs R. Glaisher and M. O'Keeffe for helpful advice.

Note added in proof: The use of eigenvalue perturbation theory for absorption in acentric crystals is an approximation. See Bird, James & King [*Phys. Rev. Lett.* (1989), **63**, 1118]. The sign of the phase triplet may be determined as described by Marthinsen & Høier [*Proc. EMSA*, (1989), p. 484].

References

BETHE, H. A. (1928). *Ann. Phys. (Leipzig)*, **87**, 55-129.
BIRD, D., JAMES, R. & PRESTON, A. R. (1987). *Phys. Rev. Lett.* **59**, 1216-1219.
CHANG, S. (1987). *Crystallogr. Rev.* **1**, 87-184.
COWLEY, J. M. (1953). *Acta Cryst.* **6**, 516-526.
COWLEY, J. M. (1981). *Diffraction Physics*, 2nd ed. New York: North-Holland.
FOX, A. G. & FISHER, R. M. (1988). *Aust. J. Phys.* **41**, 461.
FUES, E. (1949). *Z. Phys.* **125**, 531-538.
GJØNNES, J. & HØIER, R. (1971). *Acta Cryst.* A**27**, 313-316.
GOODMAN, P. (1976). *Acta Cryst.* A**32**, 793-798.
HØIER, R. & ANDERSON, B. (1974). *Acta Cryst.* A**30**, 93-95.
HØIER, R., ZUO, J. M., MARTHINSEN, K. & SPENCE, J. C. H. (1988). *Ultramicroscopy*, **26**, 25-30.
HUMPHREYS, C. J. (1979). *Rep. Prog. Phys.* **42**, 1825-1887.
HURLEY, A. C. & MOODIE, A. F. (1980). *Acta Cryst.* A**36**, 737-738.
International Tables for X-ray Crystallography (1974). Vol. IV, edited by J. A. IBERS & W. C. HAMILTON, Tables 2.2A and 2.4.6A. Birmingham: Kynoch Press. (Present distributor Kluwer Academic Publishers, Dordrecht.)
KAMBE, E. (1957). *J. Phys. Soc. Jpn*, **12**, 1-13
KOGISO, M. & TAKAHASHI, H. (1977). *J. Phys. Soc. Jpn*, **42**, 223-231.
LEWIS, A. L., VILLAGRANA, R. E. & METHERELL, A. J. F. (1978). *Acta Cryst.* A**34**, 138-139.
MARTHINSEN, K. & HØIER, R. (1986). *Acta Cryst.* A**42**, 484-492.
MARTHINSEN, K. & HØIER, R. (1988). *Acta Cryst.* A**44**, 558-562.
MARTHINSEN, K., MATSUHATA, H., HØIER, R. & GJØNNES, J. (1988). *Austr. J. Phys.* **41**, 449.
MATSUHATA, H., TOMOKIYO, Y., WATANABE, Y. & EGUCHI, T. (1984). *Acta Cryst.* B**40**, 544-548.
MIYAKE, S. & UYEDA, R. (1955). *Acta Cryst.* **8**, 335-342.
SAXTON, O., O'KEEFFE, M. A., COCKAYNE, D. J. & WILKENS, M. (1983). *Ultramicroscopy*, **12**, 75-79.
SELLAR, J. R., IMESON, D. & HUMPHREYS, C. J. (1980). *Acta Cryst.* A**36**, 686-698.
SHISHIDO, T. & TANAKA, N. (1976). *Phys. Status Solidi A*, **383**, 453-457.
SMART, D. J. & HUMPHREYS, C. J. (1978). *Inst. Phys. Conf. Ser.* **41**, 145-148.
SPENCE, J. C. H. & ZUO, J. M. (1988). *Rev. Sci. Instrum.* **59**, 2102.
STEVENSON, A. W., MILANKO, M. & BARNEA, Z. (1984). *Acta Cryst.* B**40**, 521-525.
TAFTØ, J. & GJØNNES, J. (1985). *Ultramicroscopy*, **17**, 329-335.
VINCENT, R., BIRD, D. & STEEDS, J. W. (1984). *Philos. Mag.* A**50**, 765-778.
VOSS, R., LEHMPFUHL, G. & SMITH, D. (1980). *Z. Naturforsch.* **59**, 973-984.
ZUO, J. M., GJØNNES, K. & SPENCE, J. C. H. (1989). *J. Electron Microsc. Tech.* **12**, 29-55.
ZUO, J. M., SPENCE, J. C. H. & HØIER, R. (1989). *Phys. Rev. Lett.* **62**, 547-550.
ZUO, J. M., SPENCE, J. C. H. & O'KEEFFE, M. (1988). *Phys. Rev. Lett.* **61**, 353-357.

Acta Cryst. (1989). A**45**, 851-861

Segmented Anisotropic Refinement of Bovine Ribonuclease A by the Application of the Rigid-Body TLS Model

BY BRENDAN HOWLIN,* DAVID S. MOSS AND GILLIAN W. HARRIS†

Department of Crystallography, Birkbeck College, Malet Street, London WC1 7HX, England

(*Received* 4 *October* 1988; *accepted* 7 *August* 1989)

Abstract

The anisotropic displacements of selected rigid groups in bovine ribonuclease A have been refined from X-ray diffraction data by the application of the rigid-body **TLS** model. The rigid groups chosen were the side chains of tyrosine, histidine and phenylalanine and the planar side chains of aspartic acid, glutamic acid, glutamine, asparagine and arginine. The method has also been applied to the co-crystallizing active-site sulfate anion. This has enabled the description of the motion of the above-mentioned side-chain atoms by anisotropic displacement ellipsoids from a 1·45 Å refinement. The hydrophobic side

* Present address: Department of Chemistry, University of Surrey, Guildford GU2 5XH, England.
† Present address: AFRC Institute of Food Research, Reading Laboratory, Shinfield, Reading RG2 9AT, England.

0108-7673/89/120851-11$03.00